

Mechanical and dielectric characterization of hemp fibre reinforced polypropylene (HFRPP) by dry impregnation process

B. Kechaou¹, M. Salvia², B. Beaugiraud², D. Juvé², Z. Fakhfakh¹, D. Treheux^{2*}

¹Laboratoire des Matériaux Composites Céramiques et Polymères, Faculté des Sciences de Sfax (3018), Tunisia

²Laboratoire de Tribologie et Dynamique des Systèmes UMR CNRS 5513, Ecole Centrale de Lyon 69134 ECULLY Cedex, France

Received 14 October 2009; accepted in revised form 14 January 2010

Abstract. Natural fibres such as jute, coir, sisal, bamboo and pineapple are known to have high specific strength and can be effectively used in composites in various applications. The use of hemp fibres to reinforce the polymer aroused great interest and expectations amongst scientists and materials engineers. In this paper, composites with isotactic polypropylene (iPP) matrix and hemp fibres were studied. These materials were manufactured via the patented FIBROLINE process based on the principle of the dry impregnation of a fibre assembly with a thermoplastic powder (iPP), using an alternating electric field. The aim of this paper is to show the influence of fibre/matrix interfaces on dielectric properties coupled with mechanical behaviours. Fibres or more probably the fibre/matrix interfaces allow the diffusion of electric charges and delocalise the polarisation energy. In this way, damages are limited during mechanical loading and the mechanical properties of the composites increase. The structure of composite samples was investigated by X-ray and FTIR analysis. The mechanical properties were analysed by quasistatic and dynamic tests. The dielectric investigations were carried out using the SEMME (Scanning Electron Microscope Mirror Effect) method coupled with the measurement of the induced current (ICM).

Keywords: *polymer composites, hemp, iPP, mechanical properties, electrical properties*

1. Introduction

It is now proven that natural fibres are excellent reinforcements for composite materials. Economic and environmental reasons have generated increasing interest to use ligno-cellulosic fibres in composite systems. New environmental legislation as well as consumer pressure have forced manufacturing industries (particularly automotive, construction and packaging) to look for new materials that can substitute conventional reinforcing materials, which are non-renewable, such as glass fibre [1]. The main advantages of natural plant fibres compared to traditional glass fibres are economical viability, low density, reduced tool wear, enhanced energy recovery, reduced dermal irritation, reduced

respiratory irritation and good biodegradability. Moreover these reinforcements [2–5] can reach mechanical properties such as specific strength and modulus comparable with glass fibres. Recently, natural fibres have been used to reinforce traditional thermoplastic polymers, especially polypropylene in automotive applications [6–12].

As for fibre reinforced composites, the interfacial zone plays a leading role in load transfer between fibre and matrix and consequently in the mechanical properties such as strength. Different previous studies, which focused on model or technical insulating materials, show the effect of the electric charges on the dielectric properties (such as breakdown etc.) on the mechanical properties (such as

*Corresponding author, e-mail: daniel.treheux@ec-lyon.fr
© BME-PT

friction, wear, fracture etc.) of ceramics and polymers [13–16]. In fact, both mechanical and dielectric catastrophic effects could be due to the trapping-detrapping of electric charges on intrinsic or extrinsic structural defects [13, 14]. Previous papers have shown the significant role of the fibre/matrix interface (glass fibre *E*/epoxy matrix), on the motion of the electric charges related to the interface nature: a material that favours the diffusion of electric charges along interfaces has better mechanical and tribological properties [17, 18].

In this study, this approach is applied and focuses on composites with isotactic polypropylene (iPP) organic matrix reinforced by hemp natural fibres, fabricated by a new dry impregnation process.

2. Materials and techniques

2.1. Materials

These materials were manufactured via the patented FIBROLINE [19] process that has been based on the principle of the impregnation of a fibre assembly (dried or not dried) with a thermoplastic powder (iPP), using an alternating electric field. This process was developed in co-operation by FIBROLINE (France) and IFTH (Institut Français du Textile et d'Habillement) Lyon, France.

The application of an alternating voltage produced by electrodes creates ions between the two dielectric ones and forms plasma. These ions enter in collision with the polypropylene powder particles and charge them electrically. Following complex physical phenomena, the modification of the surface of the hemp fibres and the IPP powders can occur, that could induce an improvement of the adherence on the matrix. Ultra high fluidity iPP of Lyondell-Basell group (Moplen HP500V) with melt flow rate (MFR) of 120 g/10 min is used. The polymer pellets are micronized. The micronized powder average diameter is in the range 50–200 μm .

Before impregnation, the fibres have the form of a randomly dispersed 'non-woven (mat)' in the plane without any privileged orientation in the plane. The mat is provided by IFTH (Institut Français du textile et de l'habillement). The average diameter and length of the fibre are 26 μm and 25 mm, respectively. Two batches of composites were manufactured by Fibroline using the specific process developed by IFTH. Following preliminary tests, the 30% average fibre volume fraction was chosen

to be in the range of classical short fibre GFRP density used in automotive industry (weight fraction around 40%). In this study, three samples were studied: the polypropylene (PP) matrix, composite with PP matrix and dried hemp fibre (C_D), composite with PP matrix and not dried hemp fibre (C_{ND}). For composite named C_D , the mat was dried for 72 h at a temperature of 60°C for one batch (dry) and immediately impregnated after drying. For the other system (C_{ND}) the reinforcement was used as received. The humidity content of the fibre before drying is 4%. The immediate impregnation after drying makes impossible the measurement of exact hemp humidity after drying, but the weight loss is very weak. In both cases, fibres did not receive any specific interface treatment. All the samples were taken directly in the plates 1 or 2 mm thick,

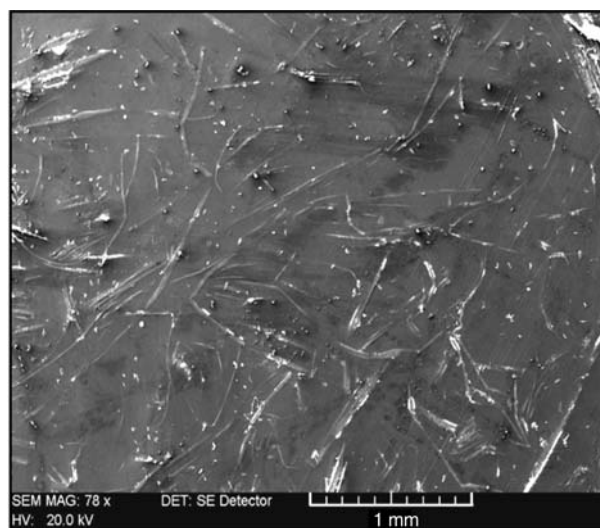


Figure 1. Microscopic observation (SEM) of the surface (C_D or C_{ND})

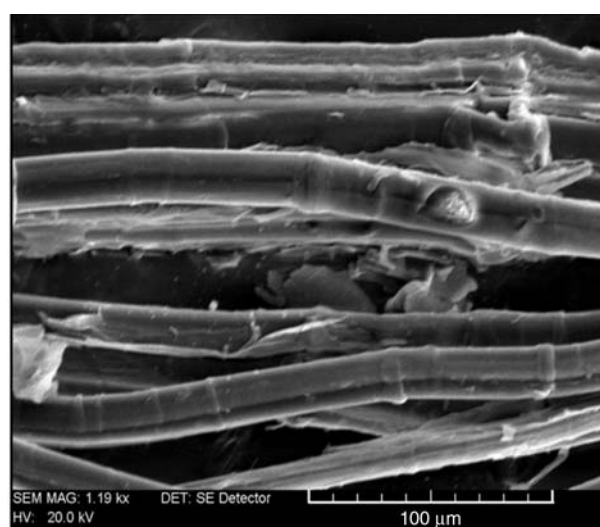


Figure 2. Microscopic observation (SEM) of the shape of the hemp fibres

obtained after the impregnation, without machining of surface.

Figure 1 presents SEM pictures to the surface of the sample that show the random distribution of the fibre. The shape of the hemp fibres is given in Figure 2.

2.2. Characterization methods

Physicochemical characterizations by FTIR and X-ray were carried out for comparing the structure of our composites, obtained by dry impregnation, with the results of the literature which use traditional processes.

2.2.1. Infra-red spectroscopy (FTIR)

The spectra were obtained with a Perkin-Elmer spectrum one FT-IR spectrometer working in Attenuated Total Reflectance mode (ATR) performing a total of 8 scans and having a resolution of 4 cm^{-1} . All ATR spectra were plotted in transmittance vs. wave number. The analyzed zone is 3 mm^2 .

2.2.2. X-ray diffraction (WAXS)

X-ray diffraction analyses of materials were performed at room temperature by using a Nonius FR590 diffractometer (operating at 30 kV and 15 mA) with a $\text{CuK}\alpha$ monochromatic radiation ($\lambda_{\text{K}\alpha} = 0.154\text{ nm}$). The scans were achieved within a range from 5 to 50° (2θ) with a scanning step of 0.03° in symmetrical geometry (Bragg-Brentano configuration). The spot size was about 10 mm high and 1 mm wide.

2.2.3. Dynamic Mechanical Analysis (DMA)

Dynamic mechanical tests were carried out with a DMA 50 analyzer from 01 dB-Metravib working in the tension-compression mode. The value of 0.01% for the strain magnitude was chosen that is in the linear domain of viscoelasticity of the material. The samples were thin rectangular strips that have dimensions of about $(35 \times 5.8 \times 1)\text{ mm}^3$. Measurements were performed in isochronal conditions at 10 Hz, at a rate of $2^\circ\text{C}/\text{min}$ and the temperature range is -100 and 130°C . This setup measured the complex tensile modulus E^* , i.e. the storage, E' ,

and the loss, E'' , as well as their ratio (E''/E'), i.e. $\tan\delta$.

2.2.4. Monotonous flexion test

The three-point bending monotonic tests, using an INSTRON testing machine (4300 type), allowed us to determine the apparent modulus (E), the maximum stress (σ_{max}) and the maximum strain ε_{max} [%]. The samples were about 100 mm long, 10 mm wide and 2 mm thick. The span to depth ratio (L/h) is greater than 20 in order to minimize shear stress. The tests were performed at 2 mm/min, under ambient conditions (test temperature: 23°C ; relative humidity: 50%).

2.2.5. Induced Current Method (ICM) and Scanning Electron Mirror Effect Method (SEMME)

The dielectric behaviour of insulating material is related to its aptitude to trap electric charges, i.e. to the density and energy of traps present in the material. It is also related to its capacity to diffuse electric charges without damage.

Before dielectric study, each sample was ultrasonicated in ethanol bath during 5 minutes, and dried before its introduction in the vacuum chamber of the SEM at the ambient temperature.

After the introduction of the sample into the microscope, the insulating material is charged by a focused or unfocused electron beam (LEO 440 Electron Microscopy Ltd., Cambridge, UK) during an injection time t_{inj} and a well controlled acceleration voltage V_{acc} .

Any evolution of the total electric charges in the SEM/insulating material system involves a flow of induced charges towards the ground of the SEM [20]. This evolution is recorded in the form of Induced Current I_g . This current is measured using a picoammeter (Keithley type). The curve $I_g = f(\text{times})$ permits to obtain the total quantity of charges Q_{IC} , distributed in the samples (bulk and surface) during the injection.

The injection conditions fixed for this study are: $V_{acc} = 10$ or 30 kV , $t_{inj} = 40$ or 100 ms .

The evolution of I_g during injection (Figure 3) gives information on the different steps of diffusion or trapping of charges present in the insulating sample.

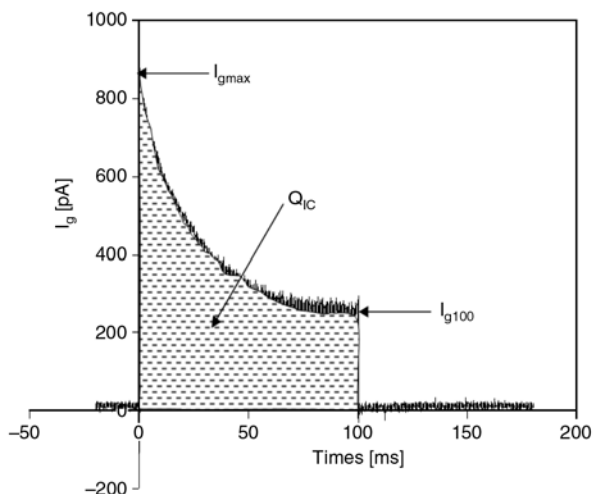


Figure 3. Parameters measured by Induced Current Method (ICM)

Different parameters can be deduced from this curve (Figure 3):

- I_{gmax} : initial current that informs on the response of material without any perturbation;
- Q_{IC} : quantity of charges distributed in the sample;
- I_{g40} or I_{g100} : value of the induced current respectively for 40 or 100 ms injection time.

The SEMME method will be performed after the injection step. The observation at lower energy ($V = 100\text{--}200\text{ V}$) of the irradiated zone makes it possible to put in evidence the mirror effect (Figure 4) [21, 22]. In fact negative charges Q_t locally trapped and stabilized near to the injection point can induce the deflection of incident electrons: the mirror image is a view of the SEM chamber. The quantity Q_t of trapped charges can be deduced from the slope of the linear part of the ‘mirror’ curve $1/d = f(V)$ according to an electrostatic law, estab-

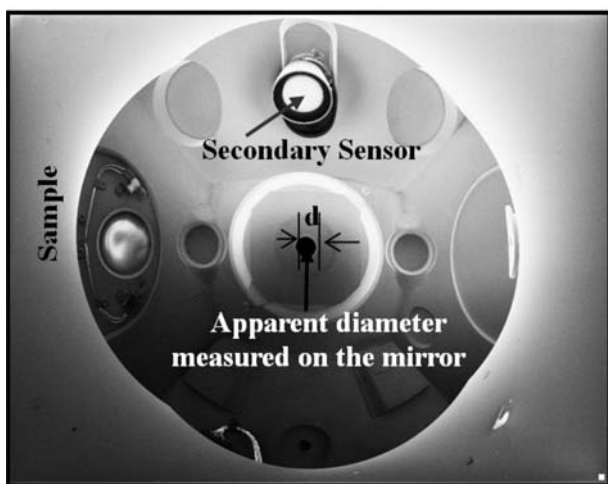


Figure 4. Mirror image

lished by Vallayer [22], relating the real diameter d' of the last output diaphragm and the apparent one, d , measured on the mirror image (Equation (1)):

$$\frac{1}{d} = \frac{4L}{d'} \cdot \frac{2\pi\epsilon_0(\epsilon_r + 1)}{K(h) \cdot Q_t} \cdot V \tag{1}$$

where L is the working distance of the SEM; d' the diameter of the last output diaphragm, d the apparent diameter measured on the mirror image, $K(h)$ a parameter dependent on SEM chamber and permittivity of the sample, and V the acceleration potential of the electron beam.

The comparison between Q_{IC} , measured by the ICM method and Q_t , measured by the mirror method, gives information of the charge state in the sample. In fact, if $Q_t/Q_{IC} = 1$, the charges are stabilized and trapped near the injection point. However, if Q_t/Q_{IC} tends towards 0, the charges diffuse in the sample from the injection point.

3. Results and discussion

3.1. Infrared spectroscopy measurements

Figure 5 shows the spectra of neat iPP matrix, hemp fiber mat as received, composite C_D and composite C_{ND} , obtained with infra-red spectrometer (FTIR) in Attenuated Total Reflectance (ATR) mode.

The neat matrix:

The isotactic polypropylene consists of propene repeating units ($\text{CH}_2\text{--CH}(\text{CH}_3)$) linked together.

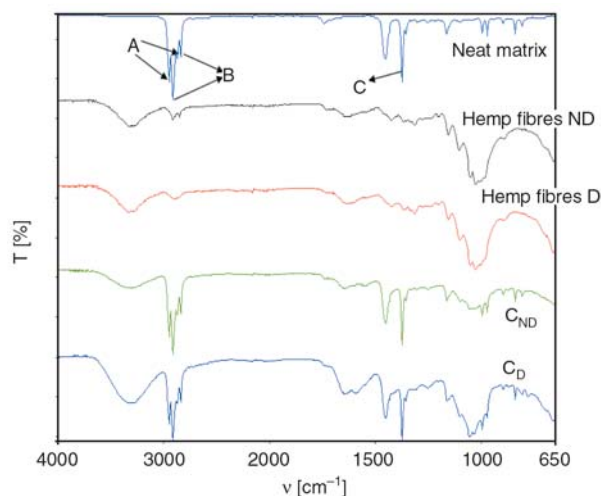


Figure 5. FTIR spectra (transmittance T vs. wave number ν) of four samples: matrix, fibre of hemp no dried and dried, C_{ND} , C_D (the scale is the same for each spectrum)

The methyl groups ($-\text{CH}_3$) are located on alternation with a hydrogen (H) in the backbone chain and are all on the same side. The peaks corresponding to the methyl group occur at 2953, 2873 and 1375 cm^{-1} (C). The two first peaks (A) are attributed to the stretch vibration asymmetric and symmetric of C–H. The last one is known as ‘umbrella’ mode (symmetric bending mode) (C). The peaks at 2913 and 2840 cm^{-1} (B) are related to methylene group (CH_2) asymmetric and symmetric C–H stretches. The peak located at 1453 cm^{-1} is due to the overlapping of the asymmetric bending mode of the (CH_3) and the methylene scissoring mode [23]. The other peaks are of less intensity, but the occurrence of the adsorption peaks at about 1160, 997, 973, and 841 cm^{-1} is in agreement with the tacticity of the polymer [24, 25]. Moreover, even though the methine groups (CH) are present in the structural unit, the peaks are not observed [23].

The hemp mat:

Hemp fibre mat was analyzed ($\%T = f(v)$) in the as received (not dry) and dry state. Plant fibre such as hemp contains cellulose (about 70%), non cellulosic polysaccharide (hemicellulose and pectin), lignin and wax. According to the literature [25], the native cellulose consists of long chain of (1-4)- β linked D-glucose units mostly aligned in parallel (cellulose I_β).

The spectra show the major bands classically observed in other ligno-cellulosic fibres. The broad and strong peak at about 3300 cm^{-1} [25] is characteristic of O–H stretching for hydrogen-bonded hydroxyl group in polysaccharides. The weak absorption peak observed at about 1730 cm^{-1} is characteristic of hemicellulose. It is attributed to carbonyl group (C=O) stretch. The weak broad peak that occurs at around 1600–1650 cm^{-1} is associated with water adsorbed in cellulose [25]. The large peak with maximum at about 1030 cm^{-1} is linked with C–O vibrations in cellulose. Finally, it appears that the absence of peak at around 1500 cm^{-1} corresponding of aromatic symmetrical stretching points out that the fibres are practically free of lignin. Probably, because of the low rate of humidity (<4%), there are no obvious differences between as received and dry mats except the peak characteristic of waxes [26] (CH_2 symmetrical stretching) at about 2850 cm^{-1} .

The composites:

The spectra of composite PP/hemp fibres (C_D or C_{ND}) are finally analyzed. These spectra show that PP matrix is modulated by the presence of hemp fibres i.e. there is no new peak appearing in the composites and thus no bond formed between the matrix and the fibres. Although the two spectra are similar, it can be noted that the amplitudes of the peaks at 3300 and 1030 cm^{-1} are higher for C_D . This phenomenon is possibly due to the fact that the surface of the C_D composite exhibits more cellulosic fibre characteristic than C_{ND} composite [27]. The literature [28, 29] reports that the volume crystallinity index is proportional to A_{841}/A_{973} ratio where A_{973} is the absorbance peak intensity at 973 cm^{-1} that is insensitive to the amorphous/crystalline ratio of isotactic polypropylene whereas A_{841} is the intensity of the band at 841 cm^{-1} linked to crystallinity content. For the neat matrix and the two composites this ratio is close and thus the crystallinity rate too.

Thus, the dry impregnation process does not modify basically the results observed classically.

3.2. X-ray analysis

Figure 6 illustrates the WAXS patterns in conventional mode (θ – 2θ) of the different samples. The peaks of semicrystalline polypropylene and an

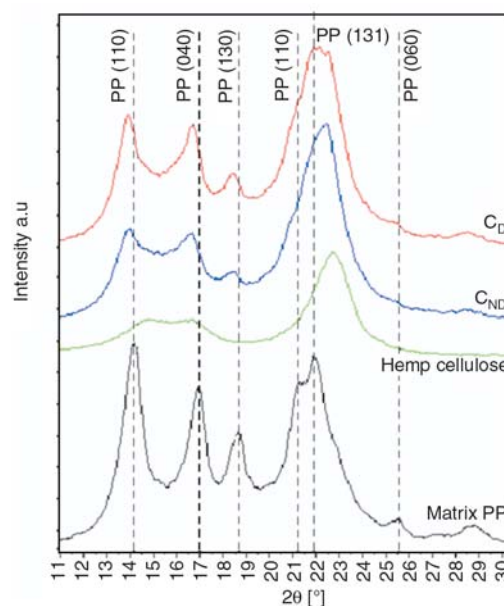


Figure 6. X-ray diffraction patterns of matrix, hemp fibres and composites. The figure is limited to the angular field presenting peaks of significant intensity.

amorphous background noise between 12 to 24° (in 2θ), were observed. These peaks, in accordance with JCPDS 00-050-2397, appear at 14.16, 17.06, 18.65, 21.34 and 21.91° (in 2θ) that are characteristics of the α -monoclinic crystal structure and corresponding to the (110), (040), (130), (111) and ($\bar{1}31$) planes, respectively. No peak occurs at $2\theta = 16^\circ$ that is characteristic of the β -hexagonal phase.

The XR diffractogram of hemp fibres shows three peaks at 15; 16.47 and 22.77° (in 2θ) corresponding to the ($1\bar{1}0$), (110), (002) planes of the I_β cellulose structure [30] respectively as the cellulose is expected to be the only crystalline constituent in plant fibre. Using synchrotron radiation and neutron diffraction, Nishiyama *et al.* [31] specifies that the structure consisted of two parallel chains having slightly different conformations and organized in sheets packed in a ‘parallel-up’ fashion, with all hydroxymethyl groups.

For composites, the presence of hemp fibres modulated the PP diffractograms. As for neat matrix, no hexagonal phase (β) is detected. Indeed β -hexagonal form could appear in HFRPP according to the processing [12]. The broad peak at $2\theta \sim 22.5^\circ$ is due to the overlapping of the diffraction peaks of the PP-crystals at $2\theta = 21.34$ and 21.91° with the peak of the cellulose-crystals at $2\theta = 22.77^\circ$. The incorporation of hemp fibres involves a shift to lower 2θ of the other polypropylene peaks that corresponds to a modification of the lattice parameters of the monoclinic α phase of the polypropylene matrix, most probably due to internal stress.

3.3. Dynamic mechanical thermal properties

Experimental results of mechanical dynamic tests, are represented in Figures 7 (loss factor $\tan\delta$) and 8 (tensile storage modulus E') for the neat matrix and the two composites at 10 Hz.

The three classical relaxations of polypropylene are observed named γ , β and α in order of increasing temperature [32]:

- Relaxation γ ($T_\gamma \sim -65^\circ\text{C}$ for neat PP) is related to the local motions in the amorphous phase.
- Relaxation β ($T_\beta \sim 10.5^\circ\text{C}$, for neat PP) is associated with the glass transition, that is to long distance molecular motions.
- Relaxation α ($T_\alpha = 100^\circ\text{C}$ for neat PP), that appears only on neat matrix spectrum is attrib-

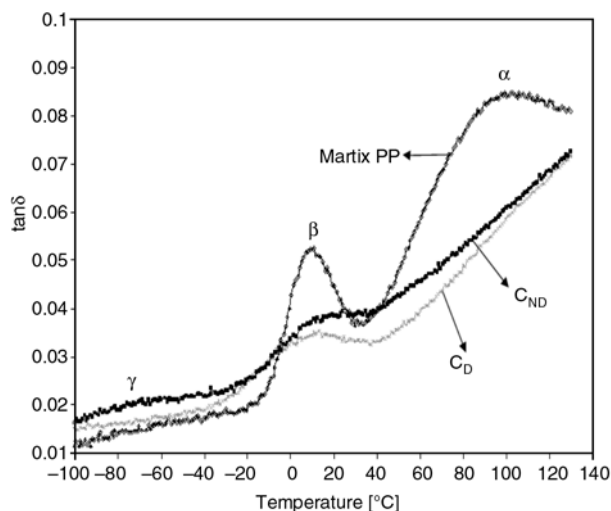


Figure 7. Mechanical loss factor $\log(\tan\delta)$ vs. temperature of the neat matrix and the two composites at 10 Hz

uted to the presence of the crystalline phase. In fact, this relaxation is not found on the curves of $\tan\delta$ of an atactic PP (amorphous) and it is known to be sensitive to modifications of crystallites by thermal or mechanical treatments (annealing, drawing). Even this relaxation is a post- T_g transition the activation energy (~ 130 kJ/mole) is lower than the activation energy of α -relaxation (~ 330 kJ/mole) and follows an Arrhenius law that implies less cooperative motion than α -relaxation. The mechanisms generally proposed for explaining this relaxation include conformational defect diffusion within the crystal, and interaction between amorphous and crystalline phases, the translation of chains in the crystal part involving modification of chain segments at the interface between the two phases [32, 33].

The incorporation of the hemp fibres increases the storage modulus of the matrix whatever the temperature range. Indeed the modulus of composite is determined by the moduli of the constituents (fibre and matrix) but also by the fibre-matrix interaction especially in the case of off-axis and randomly oriented fibre composite. The slightly higher increase of modulus for composites with dried fibres suggests improved adhesion between fibre and matrix probably due to better wetting associated to the wax removal, leading to the slightly better transfer of stress from matrix to the fibre in the case of composite with dried fibre. In fact, the modulus of the fibre is about the same whatever the treatment

(50 GPa [19]). The effect of fibre-matrix adhesion on tensile modulus of such composites has been already experimentally shown in different studies [34, 35] but this factor is generally not taken into account for in the classical models [36] for which a perfect interface is considered. Therefore, the DMA results seem to indicate a medium adhesion at the interface.

Moreover as shown by Figure 7, the intensity of the β -relaxation is lowered in the composites compared to the neat matrix and a slight shift in peak temperature of the β -relaxation can be observed towards higher temperatures ($T_\beta \approx 10.5^\circ\text{C}$ for the matrix and $\approx 15.5^\circ\text{C}$ for the composites). These behaviours cannot be attributed to an increase in crystallinity of PP matrix since IR results indicated no major modification in crystallinity index with reinforcement. That is probably related to the reduction in the molecular mobility due to the reinforcing effect of the fibres that indicates the applied stresses are expected to be easily transferred from the matrix. The decrease of the amplitude of the relaxation associated to the glass temperature is more important for C_D composite that is consistent with enhanced polymer-fibre interaction. Hence, the non-appearance of the α -relaxation peak in the $\tan\delta$ spectra of the composites in the studied temperature range can be related to higher constraints through the interlamellar regions linked the presence of fibres that seems to be consistent with WAXS results that suggest crystal rearrangement and internal stresses.

3.4. Monotonous flexion test

The Figure 9 shows typical flexural stress strain curves for the neat matrix and the two composites obtained from the three-point bending experiment at room conditions. Three characteristic zones are pointed out:

- A linear zone corresponding to the elastic behaviour of the material.
- A nonlinear zone associated to the appearance of the plastic deformation and damage.
- A zone of failure. In all the cases the material (neat matrix and composites) beams fail from the tensile side. It can be noted that both composites can undergo loading after the maximum stress to a large extent whereas for the neat matrix, the failure is more sudden.

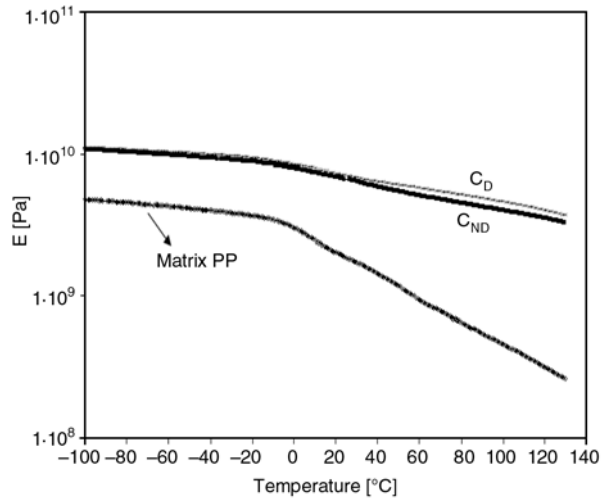


Figure 8. Tensile storage modulus (E') vs. temperature of the neat matrix and the two composites at 10 Hz

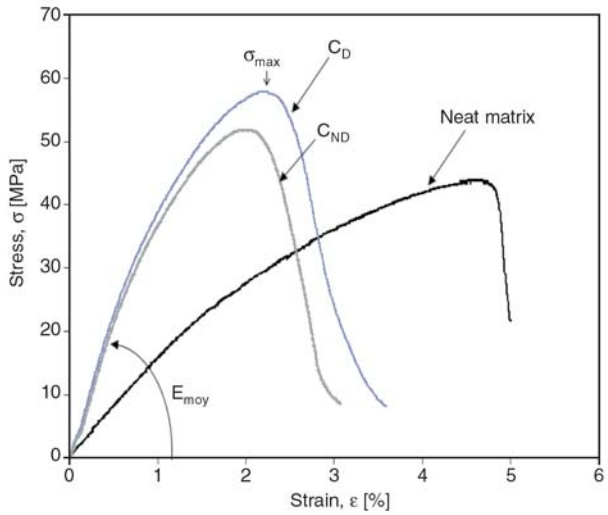


Figure 9. Typical curve of three-point bending, stress-strain for the neat matrix and the two composites at room conditions

Table 1. Flexural Mechanical properties of the tested composite materials E_{moy} apparent flexural modulus, σ_{max} and ϵ_{max} flexural stress and flexural strain respectively at maximum of the stress-strain curve (the standard deviations are in parentheses)

	E_{moy} [GPa]	σ_{max} [MPa]	ϵ_{max} [%]
Matrix	1.57 (± 0.10)	43.8 (± 1.4)	4.55 (± 0.25)
C_{ND}	4.54 (± 0.45)	51.8 (± 1.2)	2.11 (± 0.22)
C_D	4.51 (± 0.44)	56.8 (± 2.7)	2.34 (± 0.15)

The main mechanical properties determined by flexural testing are given in Table 1 (average values on five samples). Improvements in both maximum flexural stress and modulus are well noticed for the two composites.

The flexural modulus increases from 1.57 GPa for the neat polypropylene matrix to about 5.50 GPa for the composites. However, conversely to DMA

tensile storage modulus results, there is no difference within experimental scatter between flexural

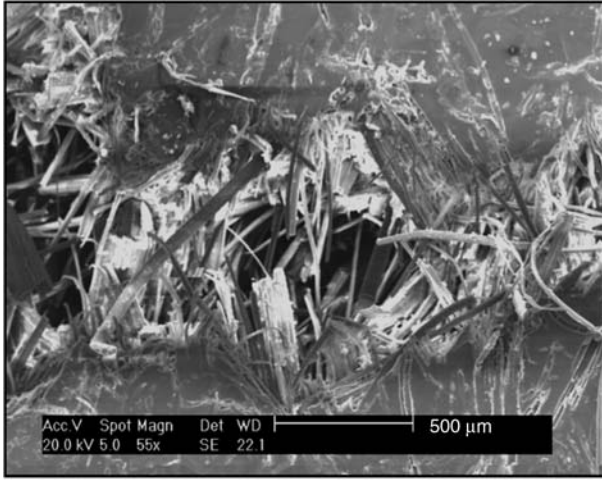


Figure 10. Examples of fracture topographies (C_{ND}) pull out and matrix rupture

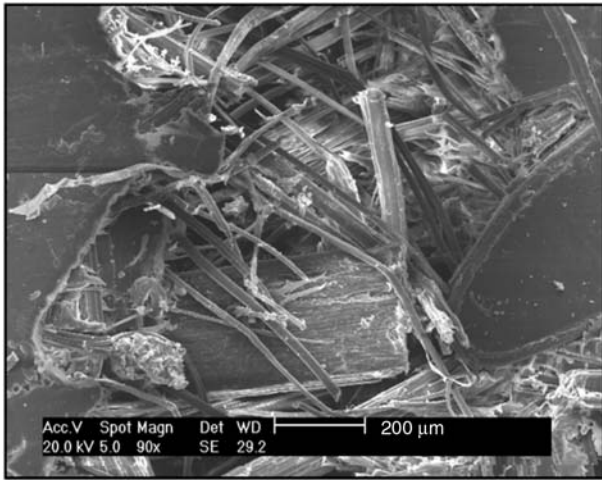
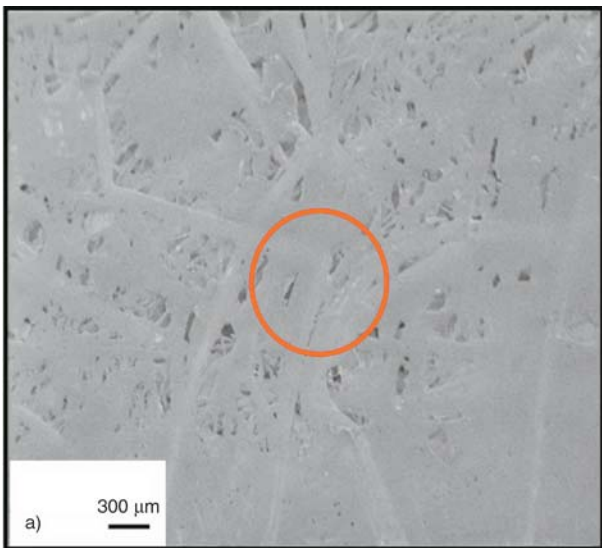


Figure 11. Fracture topography (SEM): matrix traces on fibres (C_D)



moduli of the C_D and C_{ND} composites. This result can be explained in term of the non-uniform stress distribution through thickness in the case of three-point bending loading.

The composite reinforced with dried fibres displays (C_D) slightly higher stress at maximum compared to composites made with as received fibres (C_{ND}), probably linked to an improved fibre/matrix adhesion.

SEM micrographs of typical fracture feature is given in Figures 10 (C_{ND}) and 11 (C_D). The comparative analysis of the fracture features highlights some traces of matrix remaining on the fibres after extraction (pull-out). These observations suggest a medium transfer efficiency or fibre/matrix adhesion. However the phenomenon is clearer for the composite with dried fibres (Figure 11) that is consistent with DMA results.

3.5. Mirror and Induced Current Methods (ICM)

To characterize the behaviour of the samples studied in this work, with regard to the presence of the electric charges, the ‘mirror method’ was used coupled with measurement of induced current.

In a first stage, the injection of the electrons was carried out under an accelerating voltage of 30 kV in focused mode. After injection, for low observation tension, the injected zone shows a degradation of material as proved in Figure 12 (SEM micrographs a-b).

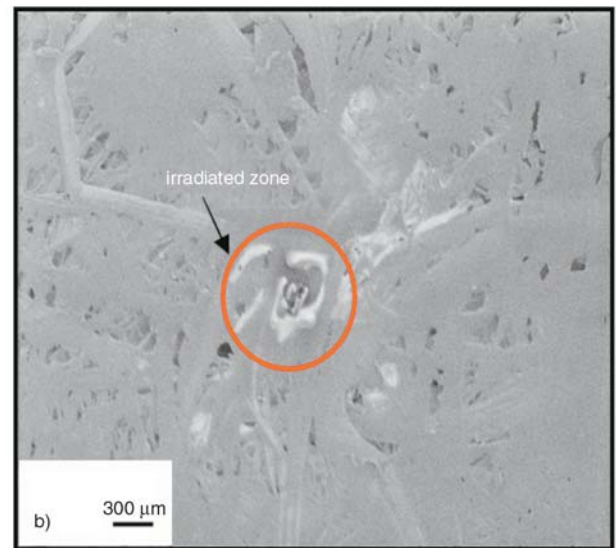


Figure 12. Total damaging of the irradiated zone (C_D or C_{ND}): (a) before injection, (b) after injection

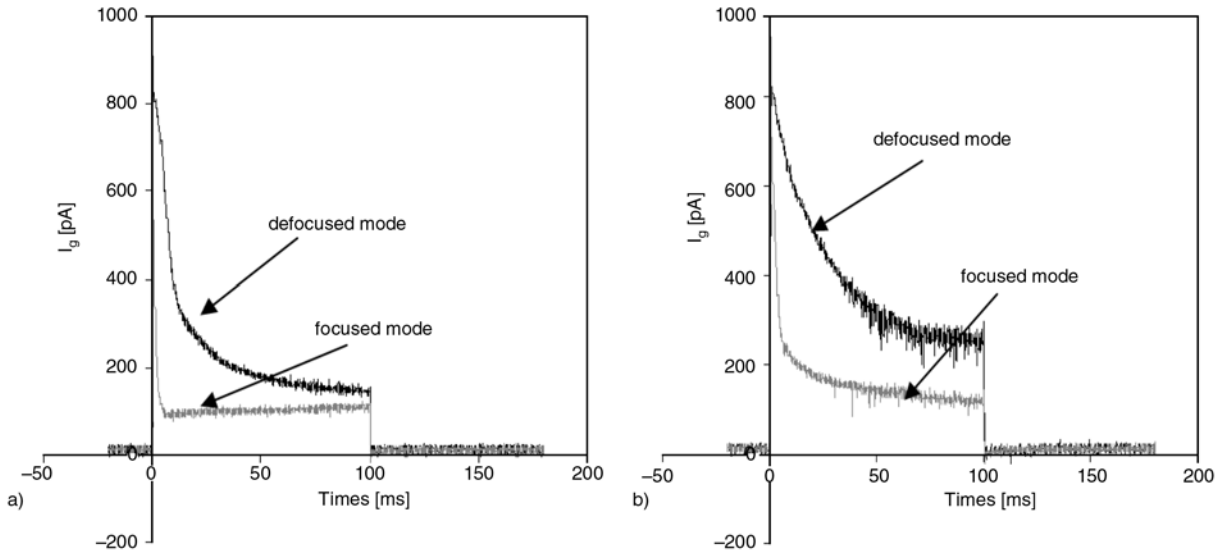


Figure 13. Curves $I_g = f(\text{time})$ in defocused or focused mode: (a) matrix PP, (b) C_D composite

For these injection conditions, a collective electric charges detrapping occurs, inducing a local destruction of the material (explosive emission) [37].

Therefore, a voltage of 10 kV was chosen, using focused or unfocused mode (diameter of injection zone: 70 μm); the injection time is 100 or 40 ms.

Figure 13 represents the ICM curves $I_g = f(\text{time})$ in defocused or focused mode for the matrix and for the C_D (similar C_{ND}).

ICM curves present the same shape in focused or defocused modes, (sharp slope of the curve at the beginning of injection and a plateau at the end of injection). However, for the defocused mode, more fibres are concerned favouring the flow of the electric charges, inducing a weaker slope at the beginning of the injection and higher current intensity at the end.

Figure 14 represents the ICM curves $I_g = f(\text{time})$ in defocused mode for the three samples: matrix PP; C_D and C_{ND} . During the injection step, some unstable micro relaxations appear (time > 50 ms) only for the C_D and C_{ND} composite (Figure 14). This phenomenon can probably protect the composite from catastrophic damages.

Consequently, following measurements were carried out using a 10 kV accelerating tension in defocused mode and $t_{inj} = 40$ ms. Figure 15 represents the evolution of the ICM current $I_g = f(\text{time})$ for the three samples and Table 2 summarizes the parameters measured by ICM and SEMME methods.

Based on ICM measurements, we can note that the incorporation of dried or not dried fibres in PP matrix increases the material capacity to store elec-

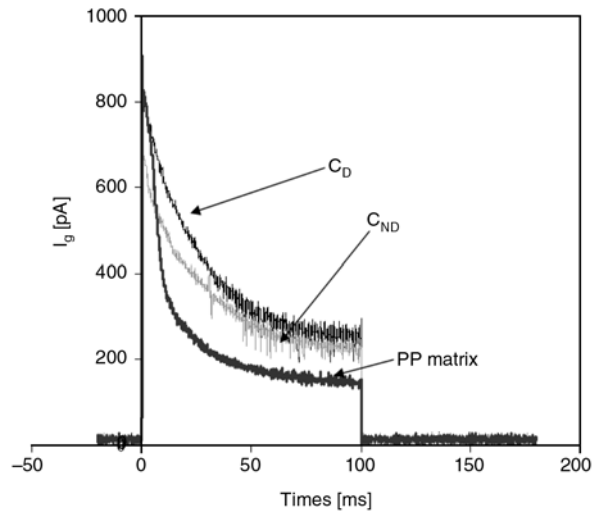


Figure 14. $I_g = f(\text{time})$ in defocused mode for the three samples, PP matrix, composite C_D and composite C_{ND} for $t_{inj} = 100$ ms

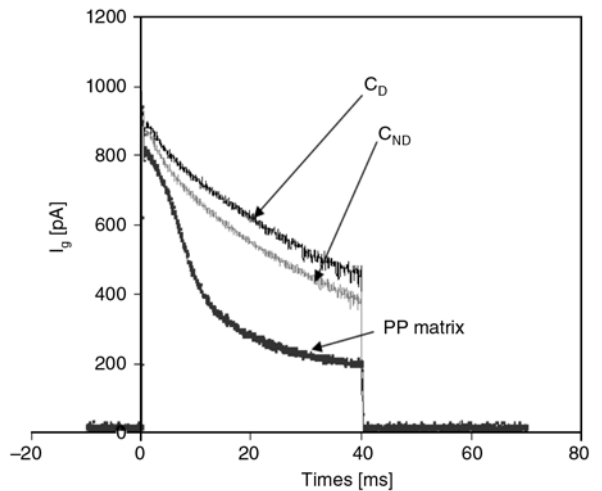


Figure 15. $I_g = f(\text{time})$ in defocused mode for the three samples, PP matrix, composite C_D and composite C_{ND} for $t_{inj} = 40$ ms

Table 2. Parameters measured according to the ICM curves and the mirror method for the three samples: matrix PP, composite C_D and composite C_{ND} for $t_{inj} = 40$ ms

	Matrix PP	C_D	C_{ND}
I_{gmax} [pA]	817 (± 9)	898 (± 10)	867
I_{g40} [pA]	206 (± 9)	435 (± 30)	406 (± 36)
Q_{IC} [pC]	14.73 (± 0.4)	25.65 (± 3)	23.31 (± 1)
Q_t [pC]	12.8 (± 0.1)	6 (± 0.1)	9.51 (± 0.1)
V_d [V]	1800	1200	1600
Q_t/Q_{IC}	0.826	0.234	0.37

tric charges (Q_{IC} composites $> Q_{IC}$ matrix), but with an easier diffusion of the charges (I_{g40} composites $> I_{g40}$ matrix) (Figure 15 and Table 2). At the beginning of the injection, the slope of the ICM curve is stronger for the matrix than for the composites and, for the matrix, the charges are more localised, near the injection zone.

Confirming the results obtained by the ICM method, the observation at low voltage, after injection of electrons, shows stable mirror images. Figure 16 represents the mirror curves $1/d = f(V)$, for the three materials. The potential V_d of disappearance of the mirror is 1200 V for the two composites (outspread of electric charges) as opposed to (1800 V) for the matrix (electric charges remains more stable and localised). This can, also, be deduced by the ratio Q_t/Q_{IC} that represents the stability of the charges which decrease under the effect of incorporating fibres in the PP matrix

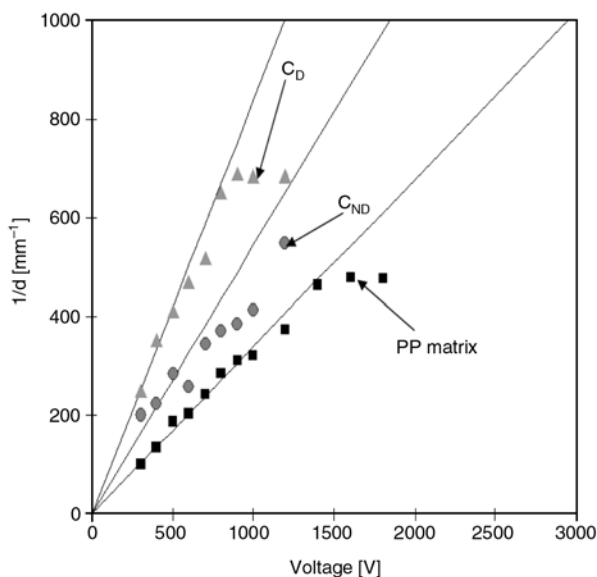


Figure 16. $1/d = f(V)$ for the three samples, PP matrix, composite C_D and composite C_{ND} for $t_{inj} = 40$ ms

(Table 2). The comparison between the dielectric measurements (Table 2) shows that the composites presents high aptitude to spreading of the electric charges (high current at the end of the injection, faster disappearance of the mirror image and Q_t/Q_{IC} weak) compared to the matrix. We can think that the incorporation of fibres or the creation of the fibre/matrix interface supports this phenomenon of delocalization of the charges and, consequently, the reduction in the polarization energy. Such a phenomenon has the effect of increasing the mechanical properties as seen previously for composites with epoxy matrix reinforced with glass fibres E [18].

In addition, a drying of fibres before the introduction into the composite is favourable. But, the observed difference remains weak compared to the composites including not dried fibres.

4. Conclusions

This work enabled us to confirm the correlation between dielectric behaviour and mechanical properties of polymers reinforced by natural fibres.

Several techniques are used to characterize the samples and the fibre/matrix interface:

- From FTIR analysis, it can be concluded that there is no chemical bond formed between the matrix and the fibres, and that the crystallinity rate is similar for neat PP and composites.
- X-ray diffraction analysis of materials shows that the presence of hemp fibres modifies the lattice parameter of polypropylene in composite materials due to internal stresses.
- As for continuous E-glass fibres [18], tests performed on hemp fibre reinforced composites prove that hems fibres modify the dielectric response of the polymeric matrix. The fibres, or more probably the fibres/matrix interfaces, allow a diffusion of the electric charges which delocalizes the polarization energy. The drying of fibres is well differentiated by IR, X-ray, ICM and SEMME methods, because the drying modifies the fibre/matrix interface and, then the trapping and/or the motion of the electric charges.
- Consequently, from the mechanical point of view, the drying of fibres is beneficial since it reinforces the fibres/matrix load transfer which, in addition, favours the diffusion of the electric charges.

In conclusion we see that it is possible to modify the characteristic of composite by the nature of fibre and the interfaces.

Acknowledgements

The authors particularly thank Eric Forest and Laurence Caramaro for the Fibroline Company for the fabrication of the samples used in this study.

References

- [1] Lee N-J., Jang J.: The effect of fibre-content gradient on the mechanical properties of glass-fibre-mat/polypropylene composites. *Composites Science and Technology*, **60**, 209–217 (2000).
DOI: [10.1016/S0266-3538\(99\)00122-0](https://doi.org/10.1016/S0266-3538(99)00122-0)
- [2] Bledzki A. K., Gassan J.: Composites reinforced with cellulose base fibres. *Progress in Polymer Science*, **24**, 221–274 (1999).
DOI: [10.1016/S0079-6700\(98\)00018-5](https://doi.org/10.1016/S0079-6700(98)00018-5)
- [3] Leao A. L., Rowell R., Tavares N.: Applications of natural fibres in automobile industry in Brazil – Thermoforming process. in ‘Science and technology of polymers and advanced materials, emerging technologies and business opportunities’ (eds.: Prasad P. N., Mark J. E., Kandil S. H.: Kafafi Z.) Plenum Press, New York, 755–761 (1998).
- [4] Robson D., Hague J., Newman G., Jeronomidis G., Ansell M.: Survey of natural materials for use in structural composites as reinforcement and matrices. Woodland Publishing Ltd., Abingdon (1996).
- [5] Mohanty A. K., Misra M., Hinrichsen G.: Biofibres, biodegradable polymers and biocomposites: An overview. *Macromolecular Materials and Engineering*, **276–277**, 1–24 (2000).
DOI: [10.1002/\(SICI\)1439-2054\(20000301\)276:1<1::AID-MAME1>3.0.CO;2-W](https://doi.org/10.1002/(SICI)1439-2054(20000301)276:1<1::AID-MAME1>3.0.CO;2-W)
- [6] Wötzel K., Wirth R., Flake M.: Life cycle studies on hemp fibre reinforced component and ABS for automotive parts. *Die Angewandte Makromolekulare Chemie*, **272**, 121–127 (1999).
DOI: [10.1002/\(SICI\)1522-9505\(19991201\)272:1<121::AID-APMC121>3.0.CO;2-T](https://doi.org/10.1002/(SICI)1522-9505(19991201)272:1<121::AID-APMC121>3.0.CO;2-T)
- [7] Riedel U., Nickel J.: Natural fibre-reinforced biopolymers as construction materials-new discoveries. *Die Angewandte Makromolekulare Chemie*, **272**, 34–40 (1999).
DOI: [10.1002/\(SICI\)1522-9505\(19991201\)272:1<34::AID-APMC34>3.0.CO;2-H](https://doi.org/10.1002/(SICI)1522-9505(19991201)272:1<34::AID-APMC34>3.0.CO;2-H)
- [8] Peijs T.: Composites for recyclability. *Materials Today*, **6**, 30–35, April (2003).
DOI: [10.1016/S1369-7021\(03\)00428-0](https://doi.org/10.1016/S1369-7021(03)00428-0)
- [9] Zah R., Hischier R., Leao A. L., Braun I.: Curauá fibers in the automobile industry – A sustainability assessment. *Journal of Cleaner Production*, **15**, 1032–1040 (2007).
DOI: [10.1016/j.jclepro.2006.05.036](https://doi.org/10.1016/j.jclepro.2006.05.036)
- [10] IENICA Summary report for European Union- Fibre crops. August (2000).
- [11] Lovins A. B., Cramer D. R.: Hypercars, hydrogen, and the automobile transition. *International Journal of Vehicle Design*, **35**, 50–85 (2004).
DOI: [10.1504/IJVD.2004.004364](https://doi.org/10.1504/IJVD.2004.004364)
- [12] Pauksza D., Borysiak S.: Structure of isotactic polypropylene in composites with natural fibres obtained in various processing methods. *Fibres and Textiles in Eastern Europe*, **13**, 107–109 (2005).
- [13] Blaise G., Le Gressus C.: Charge trapping-detrapping processes and related breakdown phenomena. in ‘High voltage vacuum insulation’ (ed.: Latham R.) Academic Press, London, 330–338 (1995).
- [14] Berriche Y., Vallayer J., Trabelsi R., Tréheux D.: Severe wear mechanisms in Al₂O₃-AlON ceramic composites. *Journal of the European Ceramic Society*, **20**, 1311–1318 (2000).
DOI: [10.1016/S0955-2219\(99\)00294-0](https://doi.org/10.1016/S0955-2219(99)00294-0)
- [15] Berroug A., Fayeulle S., Hamzaoui B., Tréheux D., Le Gressus C.: Effect of X-irradiation and friction on the properties of insulators. *IEEE Transactions on Electrical Insulation*, **28**, 528–534 (1993).
DOI: [10.1109/14.231535](https://doi.org/10.1109/14.231535)
- [16] Guerret-Piécourt C., Vallayer J., Juvé D., Tréheux D.: Limitation induced by electrical charges effects on micromechanisms. *Wear*, **254**, 950–958 (2003).
DOI: [10.1016/S0043-1648\(03\)00299-0](https://doi.org/10.1016/S0043-1648(03)00299-0)
- [17] Kchaou B., Turki C., Salvia M., Fakhfakh Z., Tréheux D.: Dielectric and friction behaviour of unidirectional glass fibre reinforced epoxy (GFRE). *Wear*, **265**, 763–771 (2008).
DOI: [10.1016/j.wear.2008.01.015](https://doi.org/10.1016/j.wear.2008.01.015)
- [18] Kchaou B., Turki C., Salvia M., Fakhfakh Z., Tréheux D.: Role of fibre-matrix interface and fibre direction on dielectric behaviour of epoxy composites. *Composites Science and Technology*, **64**, 1467–1475 (2004).
DOI: [10.1016/j.compscitech.2003.10.016](https://doi.org/10.1016/j.compscitech.2003.10.016)
- [19] Bouzouita S., Salvia M., Ben Daly H., Forest E.: Hemp/polypropylene composites. Effects of fibre treatment on fibre and fibre/matrix interface mechanical properties (in French). *Revue des Composites et des Matériaux Avancés*, **19**, 25–38 (2009).
DOI: [10.3166/rcma.19.25-38](https://doi.org/10.3166/rcma.19.25-38)
- [20] Temga T., Juvé D., Tréheux D., Guerret-Piécourt C., Jardin C.: Conduction and trapping of electric charges in an anisotropic material after irradiation with an electron beam: Application to TiO₂ single-crystal. *Nuclear Instruments and Methods in Physics Research B: Beam Interactions with Materials and Atoms*, **245**, 519–527 (2006).
DOI: [10.1016/j.nimb.2005.11.151](https://doi.org/10.1016/j.nimb.2005.11.151)

- [21] Attard C., Bigarré J., Hourquebie P.: Determination of the spatial distribution of trapped charges in insulators: Application of the electrostatic mirror method to polymers. in 'Proceeding of the 2nd Conference of Electrostatics. Montpellier, France' 77–83 (2000).
- [22] Vallayer B., Blaise G., Tréheux D.: Space charge measurement in a dielectric material after irradiation with 30 kV electron beam: Application to single-crystals oxide trapping properties. *Review of Scientific Instruments*, **70**, 3102–3112 (1999). DOI: [10.1063/1.1149887](https://doi.org/10.1063/1.1149887)
- [23] Smith B. C.: *Infrared spectral interpretation*. CRC Press, Boca Raton (1999).
- [24] Klopffer W.: *Introduction to polymer spectroscopy*. Springer-Verlag, Berlin (1984).
- [25] Subramanian K., Senthil Kumar P., Jeyapal P., Venkatesh N.: Characterization of ligno-cellulosic seed fibre from *Wrightia tinctoria* plant for textile applications- An exploratory investigation. *European Polymer Journal*, **41**, 853–861 (2005). DOI: [10.1016/j.eurpolymj.2004.10.037](https://doi.org/10.1016/j.eurpolymj.2004.10.037)
- [26] Le Troëdec M., Peyratout C., Chotard T., Bonnet J-P., Smith A., Guinebretière R.: Physico-chemical modifications of the interactions between hemp fibres and a lime mineral matrix: Impacts on mechanical properties of mortars. in '10th International Conference of the European Ceramic Society, Berlin, Germany' 451–456 (2007).
- [27] Stark M. N., Matuana L. M.: Characterization of weathered wood plastic composite surfaces using FTIR spectroscopy, contact angle, and XPS. *Polymer Degradation and Stability*, **92**, 1883–1890 (2007). DOI: [10.1016/j.polymdegradstab.2007.06.017](https://doi.org/10.1016/j.polymdegradstab.2007.06.017)
- [28] Sundell T., Fagerholm H., Crozier H.: Isotacticity determination of polypropylene using FT-Raman spectroscopy. *Polymer*, **37**, 3227–3231 (1996). DOI: [10.1016/0032-3861\(96\)88466-7](https://doi.org/10.1016/0032-3861(96)88466-7)
- [29] Lamberti G., Brucato V.: Real-time orientation and crystallinity measurements during the isotactic polypropylene film-casting process. *Journal of Polymer Science Part B: Polymer Physics*, **41**, 998–1008 (2003). DOI: [10.1002/polb.10411](https://doi.org/10.1002/polb.10411)
- [30] Abou-Sekkina M. M., Saafan A. A., Sakran M. A., Ewaida M. A.: Effects of tempering time and tempering temperature of caustic mercerization on the spectral and electrical properties of Egyptian cotton fibres. *Journal of Thermal Analysis*, **31**, 791–803 (1986). DOI: [10.1007/BF01913550](https://doi.org/10.1007/BF01913550)
- [31] Nishiyama Y., Langan P., Chanzy H.: Crystal structure and hydrogen-bonding system in cellulose I β from synchrotron X-ray and neutron fiber diffraction. *Journal of the American Chemical Society*, **124**, 9074–9082 (2002). DOI: [10.1021/ja0257319](https://doi.org/10.1021/ja0257319)
- [32] Jourdan C., Cavaille J. Y., Perez J.: Mechanical relaxations in polypropylene: A new experimental and theoretical approach. *Journal of Polymer Science Part B: Polymer Physics*, **27**, 2361–2384 (1989). DOI: [10.1002/polb.1989.090271115](https://doi.org/10.1002/polb.1989.090271115)
- [33] Davies G. R., Owen A. J., Ward I. M., Gupta V. B.: Interlamellar shear in anisotropic polyethylene sheets. *Journal of Macromolecular Science Part B: Physics*, **6**, 215–228 (1972). DOI: [10.1080/00222347208224798](https://doi.org/10.1080/00222347208224798)
- [34] Di Liello V., Martuscelli E., Ragosta G., Zihlif A.: Effect of fibre surface treatment on yielding and fracture behaviour of glass fibre-polypropylene composite. *Journal of Materials Science*, **26**, 2100–2106 (1991). DOI: [10.1007/BF00549174](https://doi.org/10.1007/BF00549174)
- [35] Ségard E., Benmedakhene S., Laksimi A., Lai D.: Influence of the fibre/matrix interface on the behaviour until fracture of polypropylene reinforced with short glass fibres (in French). *Mécanique et Industries*, **6**, 479–486 (2005). DOI: [10.1051/meca:2005060](https://doi.org/10.1051/meca:2005060)
- [36] Joseph P. V., Mathew G., Joseph K., Groeninckx G., Thomas S.: Dynamic mechanical properties of short sisal fibre reinforced polypropylene. *Composites Part A: Applied Science and Manufacturing*, **34**, 275–290 (2003). DOI: [10.1016/S1359-835X\(02\)00020-9](https://doi.org/10.1016/S1359-835X(02)00020-9)
- [37] Vaisburd D. I., Tverdokhlebov S., Tukhfatullin T. A.: Critical (burst) electron emission from dielectrics, induced by injection of a dense electron beam. *Russian Physics Journal*, **40**, 1064–1082 (1997). DOI: [10.1007/BF02508942](https://doi.org/10.1007/BF02508942)